Heliyon 10 (2024) e31630

Contents lists available at ScienceDirect

Heliyon

journal homepage: www.cell.com/heliyon

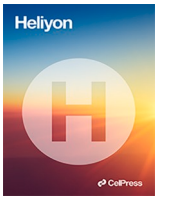

Research article

Dual dimeric interactions in the nucleic acid-binding protein Sac10b lead to multiple bridging of double-stranded DNA

Songqiang Tang [a,1], Chun-Hsiang Huang [b,1], Tzu-Ping Ko [c], Kuan-Fu Lin [a], Yuan-Chih Chang [c], Po-Yen Lin [d], Liuchang Sun [a], Chin-Yu Chen [a,*]

[a] State Key Laboratory of Biocatalysis and Enzyme Engineering, School of Life Sciences, Hubei University, Wuhan, 430062, China
[b] Protein Diffraction Group, Experimental Facility Division, National Synchrotron Radiation Research Center, Hsinchu, 30076, Taiwan
[c] Institute of Biological Chemistry, Academia Sinica, Taipei, 11529, Taiwan
[d] Institute of Cellular and Organismic Biology, Academia Sinica, Taipei, 11529, Taiwan

A B S T R A C T

Nucleoid-associated proteins play a crucial role in the compaction and regulation of genetic material across organisms. The Sac10b family, also known as Alba, comprises widely distributed and highly conserved nucleoid-associated proteins found in archaea. Sac10b is identified as the first 10 kDa DNA-binding protein in the thermoacidophile *Sulfolobus acidocaldarius*. Here, we present the crystal structures of two homologous proteins, Sac10b1 and Sac10b2, as well as the Sac10b1 mutant F59A, determined at a resolution of 1.4–2.0 Å. Electron microscopic images reveal the DNA-bridging capabilities of both Sac10b1 and Sac10b2, albeit to varying extents. Analyses of crystal packing and electron microscopic results suggest that Sac10b1 facilitates cooperative DNA binding, forming extensive bridged filaments via the conserved R58 and F59 residues at the dimer-dimer interface. Substitutions at R58 or F59 of Sac10b1 attenuate end-to-end association, resulting in non-cooperative DNA binding, and formation of small, bridged DNA segments in a way similar to Sac10b2. Analytical ultracentrifuge and circular dichroism confirm the presence of thermostable, acid-tolerant dimers in both Sac10b1 and Sac10b2. These findings attest to the functional role of Sac10b in organizing and stabilizing chromosomal DNA through distinct bridging interactions, particularly under extreme growth conditions.

1. Introduction

Chromatin proteins play an important role in packaging and organizing genomic DNA throughout all kingdoms of life. These proteins can be classified according to their architectural properties: wrapping, bending, bridging and/or stiffening DNA [1–5]. In eukaryotes, histones wrap double-stranded DNA (dsDNA) into nucleosomes [1]. In bacteria, nucleoid-associated proteins such as HU, IHF, Fis and H-NS compact the DNA by bending and bridging [2]. Archaeal nucleoid-associated proteins use strategies from both eukaryotes and bacteria. Most euryarchaea possess true histone proteins such as HMfA and HMfB that organize dsDNA into tetrameric nucleosomes [6]. Archaeal histones HTkB and HMtA2 form multimers of varied sizes with the DNA [7,8]. In a 4 Å crystal structure of archaeal histone-DNA complex, the DNA winds three histone homodimers [9]. The histone paralogue MJ1647 forms homotetramers that are capable of cooperatively bridging DNA molecules [10].

In contrast, Crenarchaea lack histone homologues. Instead, they use a wide array of small nucleoid-associated proteins to package their DNA [3–5]. The nucleoid-associated proteins of Sac10b family [11,12], characterized by their small size, basic nature and abundance, are widely distributed and highly conserved in Crenarchaea. Most genome-sequenced *Sulfolobus* species have one or two copies of Sac10b homolog, such as Sac10b1 and Sac10b2 from *Sulfolobus acidocaldarius* [13–15], Sso10b1 and Sso10b2 form

* Corresponding author.
E-mail addresses: chinyuchen33@gmail.com, chinyuchen@hubu.edu.cn (C.-Y. Chen).
[1] These authors contributed equally to this work.

https://doi.org/10.1016/j.heliyon.2024.e31630
Received 9 February 2024; Received in revised form 26 April 2024; Accepted 20 May 2024
Available online 23 May 2024

S. solfataricus [16–18], Ssh10b from *S. shibitae* [19–21] and Sis10b from *S. islandicus* [22,23]. In solution, these proteins form dimers. Sac10b1 binds to DNA duplexes with little compaction, thereby providing protection to DNA against DNase I digestion [15]. Sso10b1 engages cooperatively and non-specifically with dsDNA [16,19]. Ssh10b can restrict DNA negative supercoils at elevated temperatures [19]. During the stationary phase, Sso10b2 is expressed at 5%–10% levels of Sso10b1 [17]. Sso10b1 and Sso10b2, like Ape10b1 and Ape10b2 from *Aeropyrum pernix* [24], can form obligate heterodimers with distinct DNA-binding properties from the homodimers [16]. Electron microscopy (EM) studies reveal that Sac10b1 (or Sso10b1) can bridge two DNA duplexes and bind cooperatively along the DNA to form a filament [15,17]. Recent atomic force microscopy (AFM) investigations indicate that Sso10b1 and Sso10b2 can effectively bridge and stiffen DNA *in vitro* [25]. Consequently, the differential expression of Sso10b1 and Sso10b2 may serve as a mechanism for modulating chromatin packaging and gene expression *in vivo* [17,25].

Sac10b family proteins also interact with diverse RNA species. A recent study demonstrated that Sis10b is an RNA chaperone and functions more efficiently at elevated temperatures [23]. Sso10b1 interacts with both DNA and RNA *in vitro* but binds dsDNA more tightly [26]. The protein was released by digestion with either DNase or RNase, suggesting its associated with both nucleic acids *in vivo* [27]. Ssh10b binds with similar affinities to both DNA and RNA *in vitro*, and this protein is associated with rRNAs, mRNAs, and ribosomes in a salt-sensitive fashion *in vivo* [20].

Several crystal structures of various Sac10b homologues alone or in complex with dsDNA or dsRNA have been determined [16,17,28–35], along with two solution structures, Sso10b2 [36] and Ssh10b [21]. The Ape10b2-16 bp DNA complex reveals that Ape10b2 dimers are packed on either side of the DNA duplex in successive minor grooves [35]. It was proposed that Sac10b dimers could oligomerize because the Sac10b homolog Afu10b1 showed repeating tetramers in the crystal [32]. Importantly, Sac10b1 homologues from various species exhibit a conserved dimer-dimer interface at this interface, promoting cooperative interactions and higher-order assembly of Sac10b-nucleic acid complex [16,25,26,32,35], as shown by the site-directed mutations Afu10b1 F54R [32] and Sso10b1 F60A [26]. F60 is located at the dimer-dimer crystallographic interface of Sso10b1 and is actively involved in cooperative binding [25,26].

Sac10b stands out as the initial identification of a 10 kDa DNA-binding protein from the hyperthermophile *S. acidocaldaricus*, yet its three-dimensional crystal structure remains undetermined. Hence, we solved the crystal structures of Sac10b1 and Sac10b2 at 1.70–2.05 Å resolution to unravel the architectural differences between these two proteins. To address the physiological relevance of the dimer-dimer contacts in the crystals, mutagenesis of R58 and F59 residues in Sac10b1 was performed. Analytical ultracentrifuge (AUC) results indicate that Sac10b1, Sac10b1 F59A, and Sac10b2 exist as dimers in solution, but Sac10b1 R58A forms oligomers of various sizes in solution. The crystal structure of Sac10b1 F59A was further solved at 1.40 Å resolution. Circular dichroism (CD) spectra reveal the thermostability and acid tolerance of both Sac10b1 and Sac10b2. A previous EM study demonstrated that native Sac10b1 proteins intertwine two DNA duplexes at low protein concentrations but cooperatively bind and fully cover the DNA at high concentrations [15]. Here, we employed EM to illustrate the DNA interactions with recombinant Sac10b2, as well as the wild-type and mutant Sac10b1 proteins. Our findings support the crucial role of conserved dimer-dimer interface residues R58 and F59 at the dimer-dimer interface in facilitating cooperative binding and bridging of dsDNA.

2. Materials and methods

2.1. Protein expression and purification

The gene encoding Sac10b1 was amplified by polymerase chain reaction (PCR) from *S. acidocaldarius* genomic DNA and cloned into pET-21a vector (Novagen) using *Nde*I and *Xho*I restriction sites. The Sac10b1 containing plasmid was transformed into *Escherichia coli* BL21 Coden Plus (DE3)-RIL strain for over-expression of recombinant Sac10b1 protein. The *E. coli* cells were cultured at 37°C and induced at OD_{600} of ~0.9 for 4 h with 0.4 mM IPTG in LB medium containing ampicillin (100 μg/mL) and chloramphenicol (30 μg/mL). The cells were lysed in a binding buffer (20 mM Tris-HCl, pH7.5) by sonication, and the lysate was incubated at 65°C for 30 min to remove most of the host proteins. The protein was purified from the supernatants by using an SP cation-exchange chromatography FF column (GE Healthcare). Sac10b1 eluted at 0.7 M NaCl with a linear 0–1.0 M NaCl gradient. Fractions containing the protein were pooled and concentrated using a Centricon membrane (10 K cutoff, GE Healthcare Life Sciences).

The plasmid construction, protein overexpression and purification procedures for Sac10b2 are similar to those for Sac10b1, except the protein was eluted at 0.3 M NaCl. Site-directed mutagenesis was used to prepare two Sac10b1 mutants, R58A and F59A. The Sac10b1 F59A protein was purified using a similar method as wild-type Sac10b1, but Sac10b1 R58A cannot bind to the cation-exchange SP-column. Alternatively, the addition of 30–50% ammonium sulfate precipitated the Sac10b1 R58A protein which can be further purified by gel-filtration chromatography (Superdex G75 column, GE Healthcare). The purified recombinant proteins were analyzed by SDS-PAGE and showed high purity in Fig. S1. Protein concentrations were determined by ultraviolet absorbance at 280 nm, using extinction coefficients ε_{280} of 1490 M^{-1} cm^{-1} for Sac10b1 (and its mutants, R58A and F59A) and 7450 M^{-1} cm^{-1} for Sac10b2.

2.2. Analytical ultracentrifuge

We conducted sedimentation velocity (SV) experiments using an Optima XL-A analytical ultracentrifuge (Beckman) equipped with an An-60 Ti rotor, operating at 40,000 rpm and 20°C. The samples were prepared in a solution of 20 mM Tris-Cl at pH 7.5 and 100 mM NaCl. The protein concentrations employed for AUC analysis fell within the A_{280} absorbance range of 0.5–1.0. Specifically, they were as follows: Sac10b1 at 670 μM, Sac10b2 at 135 μM, Sac10b1 F59A at 530 μM, and Sac10b1 R58A at 400 μM. Absorbance

measurements were taken at a wavelength of 280 nm for Sac10b1, Sac10b2, and Sac10b1 F59A, as well as at a wavelength of 260 nm for Sac10b1 R58A. To determine the sedimentation coefficient and protein mass, finite element fitting of the data to a one-component system was performed using the SEDFIT software [37].

2.3. Circular dichroism

The CD spectra were acquired utilizing an Aviv Model 410 circular dichroism spectrometer with quartz cuvettes having a 1-mm pathlength. Protein samples were prepared in 20 mM sodium phosphate at pH 7.5 with a concentration of 15 μM. Far-UV CD spectra, varying with temperature, were recorded in the wavelength range of 190–260 nm with a 1 nm bandwidth at specific temperatures (25, 65, 75, 85, and 95°C). pH-dependent measurements were performed at 25°C using Na_2HPO_4/sodium citrate buffer for pH values of 3.0 and 5.0, and Na_2HPO_4/NaH_2PO_4 buffer solutions for a pH value of 7.5. Each curve represents the average of three scans.

2.4. Crystallization, data collection, and structure determination

The sitting-drop vapor diffusion method was employed for all crystallization experiments. Proteins were concentrated to 20 mg/ml in 20 mM Tris-HCl, pH 7.5 and 150 mM NaCl for crystallization. Crystallization was conducted by mixing 0.5 μl protein solution with 0.5 μl reservoir solution using a Rigaku phoenix/RE robot, and the resultant drop was equilibrated against 50 μl reservoir solution in a 96-well crystallization plate. Sac10b1 crystals were obtained by using a reservoir solution containing 0.1 M Na-acetate, pH 5.5, 0.2 M KBr and 25% PEG 2000 MME. Sac10b2 crystals were prepared by using a reservoir solution containing 0.1 M Na(OAc), pH 4.6, and 2.0 M Na-formate. Sac10b1 F59A was crystallized in the reservoir solution containing 0.1 M imidazole, pH 8.0, 20% PEG1000 and 0.2 M $Ca(OAc)_2$. Despite screening the Sac10b1 R58A protein under more than 1000 different crystal growth conditions, no evidence of crystal formation was observed. For all three proteins, rod-like crystals appeared after five days at 25°C and grew to their maximal dimension ~60 × 60 × 300 μm within two weeks.

Crystallization solution supplemented with 25% glycol was used as a cryoprotectant and crystals were mounted on a nylon loop (Hampton Research, USA) before being rapidly frozen in liquid nitrogen for subsequent data collection. X-ray diffraction data were collected for three crystals using the helical scan method and a Rayonix MX300HE CCD detector at beamline TPS 05A, National

Table 1
Data collection and refinement statistics for the Sac10b1 and Sac10b2 crystals.

	Sac10b1	Sac10b2	Sac10b1 F59A
Data collection			
Beamline	NSRRC TPS 05A	NSRRC TPS 05A	NSRRC TPS 05A
Wavelength (Å)	0.99984	0.99984	0.99984
Space group	$P6_522$	$C222_1$	$C2$
Cell dimensions			
a, *b*, *c* (Å)	81.89, 81.89, 139.37	48.25, 68.92, 173.56	95.07, 38.90, 69.12
α, β, γ (°)	90.0, 90.0, 120.0	90.0, 90.0, 90.0	90.0, 131.7, 90.0
Resolution (Å)	30.0–2.05 (2.12–2.05)	30.0–1.70 (1.76–1.70)	30.0–1.40 (1.45–1.40)
R_{merge}	0.050 (0.575)	0.056 (0.439)	0.062 (0.410)
$I/\sigma I$	39.83 (2.85)	35.22 (3.89)	17.54 (2.69)
CC1/2	0.983 (0.914)	0.965 (0.857)	0.972 (0.901)
Completeness (%)	99.9 (100.0)	99.0 (99.9)	98.4 (92.5)
Total no. unique reflections	17976 (1734)	32123 (3197)	36860 (3465)
Multiplicity	9.3 (9.0)	5.8 (5.9)	3.5 (3.0)
Refinement			
R_{work}/R_{free}	0.202/0.232	0.207/0.246	0.220/0.254
No. atoms			
Protein	1333	2077	1376
Ions	5	–	–
Water	151	234	196
B-factors (Å^2)			
Protein	29.44	40.78	21.47
Ions	31.79	–	–
Water	36.70	46.76	29.21
R.m.s.deviations			
Bond lengths (Å)	0.008	0.008	0.006
Angles (°)	0.96	1.21	0.94
Ramachandran			
Favored (%)	98.80	98.76	100.0
Outliers (%)	0	0	0
Clash score	4.28	6.34	6.61
PDB accession	8XAO	8XAP	8XAQ

Values in parentheses are for the outermost resolution shells.
Ramachandran plot was calculated by MolProbity [42], website: http://molprobity.biochem.duke.edu/.

Synchrotron Radiation Research Center in Hsinchu, Taiwan. Data processing was performed by using HKL-2000 [38]. The Sac10b1 crystal diffracted to 2.05 Å, belongs to the space group of $P6_522$, with unit-cell parameters $a = b = 81.9$ Å, $c = 139.4$ Å, and contains one dimer in the asymmetric unit. The Sac10b2 crystal diffracted to 1.7 Å, belongs to space group $C222_1$ with unit-cell $a = 48.2$, $b = 68.9$ and $c = 173.3$ Å, and contains three monomers in the asymmetric unit. The Sac10b1 F59A diffracted to 1.4 Å, belongs to the space group of $C2$, with unit-cell parameters $a = 95$ Å, $b = 38.9$ Å, $c = 69.1$ Å, and contains one dimer in the asymmetric unit. The data collection and processing statistics are shown in Table 1.

All structures were determined by molecular replacement using the program Phaser [39]. The structure of PDB 1H0X was used as a search model for Sac10b1 and Sac10b1 F59A, as well as 1UDV for Sac10b2. The structural model was further modified manually by using Coot [40] and refined by Phenix [41]. Difference Fourier (Fo-Fc) maps were calculated to locate the solvent molecules and ligands. Iterative cycles of refinement and manual rebuilding in Coot were carried out until the R_{free} value converged. R_{free} calculations were performed on 5% of the reflections. The stereochemistry of the refined structure was validated using MolProbity [42]. All φ/ψ angles and other conformational parameters in these structures are within the acceptable regions. Refinement parameters for each

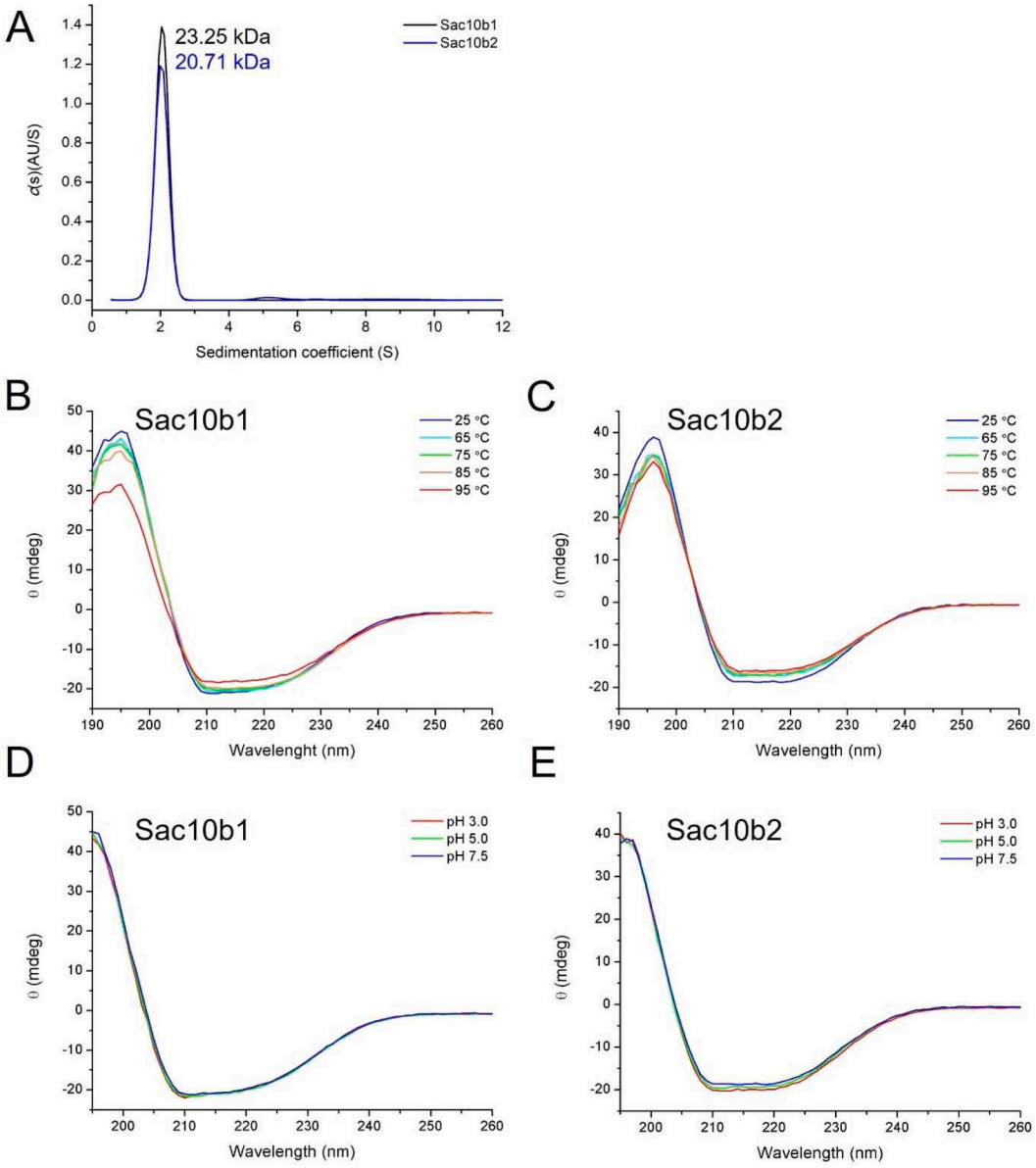

Fig. 1. Biochemical characterization of the Sac10b1 and Sac10b2 proteins. (A) The analytical ultracentrifugation sedimentation velocity profiles of the homodimers of Sac10b1 and Sac10b2 are compared. The far-UV CD spectra of Sac10b1 (B) and Sac10b2 (C) were measured over the wavelength range 190–260 nm at specific temperatures (25, 65, 75, 85 and 95°C) in 20 mM sodium phosphate buffer, pH 7.5. The far-UV CD spectra show that the secondary structure of Sac10b1 (D) and Sac10b2 (E) are unaffected by changes in pH over the range of 3.0–7.5 at 25°C.

structure are summarized in Table 1. All structural figures were prepared with PyMol (The PyMol Molecular Graphics System, Version 1.7.6.4, Schrodinger, LLC). The atomic coordinates have been deposited in the Protein Data Bank under accession code 8XAO for Sac10b1, 8XAP for Sac10b2 and 8XAQ for Sac10b1 F59A.

2.5. Electron microscopy

The phiX174 RF II DNA (New England Biolabs) is the double-stranded, nicked, circular ds-DNA molecule of 5386 bp. Sac10b-DNA complexes were formed by incubating equal volumes of ~13 nM (50 μg/ml) phiX174 DNA with 15 μM protein dimer solutions to achieve stoichiometry of 6 bp DNA per protein dimer in 20 mM Tris-Cl, pH 7.5 for 30 min at 25°C. The EM samples were prepared by the aqueous drop spreading and heavy metal shadowing methods [43,44]. In brief, a solution containing either the DNA plasmid alone or the Sac10b-DNA complex was mixed with cytochrome *c* solution (0.2 mg/mL) in 0.25 M ammonium acetate and incubated in an

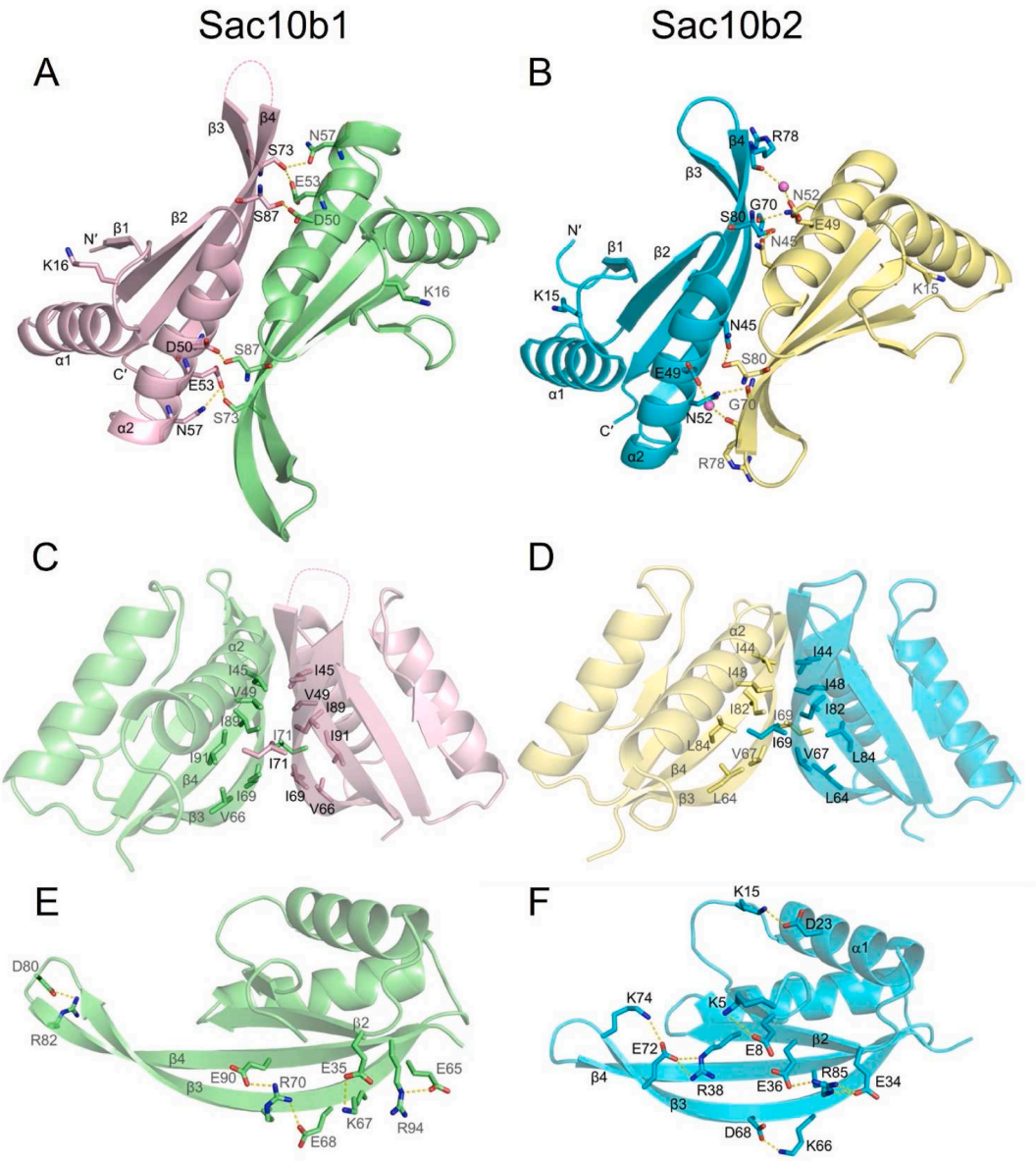

Fig. 2. Overall structures and ion-pair interactions of Sac10b1 and Sac10b2. Ribbon diagrams of the Sac10b1 dimer (A) and the Sac10b2 dimer (B) are each viewed along the molecular dyad axis (Interface I). The helices and strands are labeled α1 to α2 and β1 to β4, respectively. The subunits are colored in green and pink for Sac10b1 and in yellow and cyan for Sac10b2. The homodimer interface of Sac10b1 (C) and Sac10b2 (D) is shown in a side view and residues involved in the hydrophobic interactions are indicated. The other two ribbon diagrams show the ion-pair interactions in Sac10b1 monomer (E) and Sac10b2 monomer (F). (For interpretation of the references to color in this figure legend, the reader is referred to the Web version of this article.)

Eppendorf tube for 5 min. Subsequently, a 50-μl sample drop was placed on a clean Parafilm surface for 90 s, and a thin carbon foil-covered grid was gently touched to the surface of the drop. The grid was then rinsed with a water/ethanol series (75% ethanol for 30 s followed by absolute ethanol for 30 s), air-dried, and subjected to rotary shadowing using tungsten for contrast enhancement. The EM images were recorded at 200 kV on a Tecnai F20 Bio TWIN (FEI Co., Netherlands) using a slow-scan CCD camera (Gatan UltraScan 4000 4k x 4k, USA).

3. Results

3.1. Sac10b forms thermostable and acid-tolerant dimer in solution

AUC analysis revealed that both Sac10b1 and Sac10b2 proteins, like other homologues, exist as a dimer in solution [19,45]. Fitting of the sedimentation profiles indicated sedimentation coefficients (*S*) of 2.05 and 2.03, consistent with a mass of about 20 kDa for the Sac10b1 homodimer and Sac10b2 homodimer at micromolar concentrations (Fig. 1A). An archaeal protein from a thermoacidophile often features tolerance to heat and acidic conditions. Previously, biophysical studies have shown that Ssh10b is extremely thermal stable at the temperature of 25–90°C [19]. By comparing the CD spectra of Sac10b1 and Sac10b2 at various temperatures (Fig. 1B and C), both proteins are highly thermostable with only slight changes in CD spectra even when the temperature is elevated to 95°C. In addition, the CD spectra at 25°Cfor different pH values are almost identical (Fig. 1D and E), indicating that both proteins exhibit pH

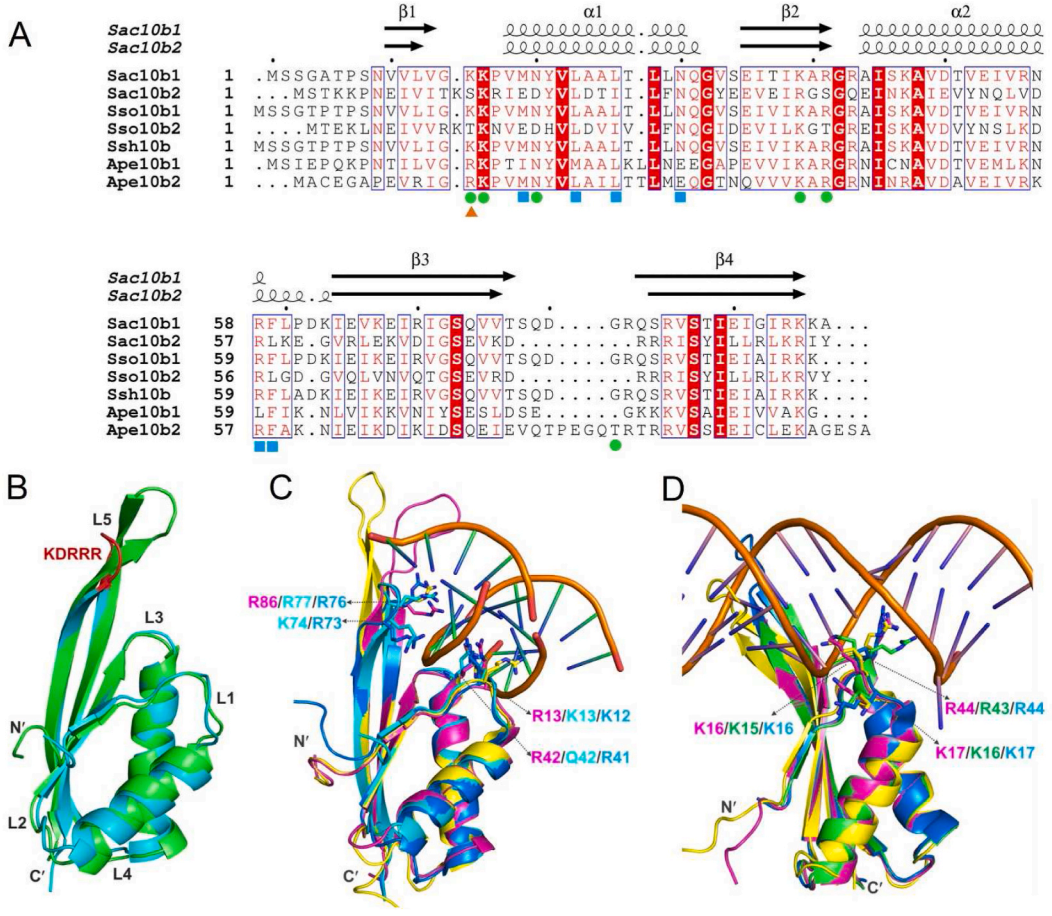

Fig. 3. Structural comparisons of Sac10b family proteins. (A) Sequence alignment of the archaeal Sac10b family proteins including Sac10b1 and Sac10b2 from *Sulfolobus acidocaldarius*, Sso10b1, and Sso10b2 from *Sulfolobus solfataricus*, Ssh10b from *Sulfolobus shibitae*, as well as Ape10b1 and Ape10b2 from *Aeropyrum pernix*. The secondary structures of Sac10b1 and Sac10b2 are displayed above the sequences. Identical residues are shown in white with a red background and conserved residues are shown in red. Residues engaged in dimer-dimer interaction, acetylation, and RNA binding are denoted by a cyan square, orange triangle, and green circle, respectively. (B) Superposition of Sac10b1 and Sac10b2. The KDRRR motif of Sac10b2 is shown in red and the five loops are labeled L1-L5. (C) Superposition of the apo-Sac10b2 structure onto the Ape10b2-dsDNA complex: Sac10b2 (8XAP, cyan, this work), Sso10b2 (1UDV, marine), Ape10b2 (2H9U, yellow) and Ape10b2-DNA complex (3U6Y, magenta). (D) Superposition of the apo-Sac10b1 structure onto the Ssh10b-dsRNA complex: Sac10b1 (8XAO, green, this work), Sso10b1 (1H0X, marine), Ssh10b (1Y9X, yellow) and Ssh10b-RNA complex (3WBM, magenta). (For interpretation of the references to color in this figure legend, the reader is referred to the Web version of this article.)

tolerance over a wide range (pH 3–7.5). Both Sac10b1 and Sac10b2 are highly thermostable and acid-tolerant proteins which are preferred in industrial use, for example, as an expression tag and to promote dimerization. The knowledge gained from these studies can be applied to engineer enzymes with enhanced stability for use in industrial processes or to design proteins with novel functions.

3.2. *The overall structures of two Sac10b proteins*

The crystal structures of both Sac10b1 and Sac10b2 monomers adopt a β1-α1-β2-α2-β3-β4 topology and have a similar IF3-like fold to their homologues (Fig. 2A and B). Five loops, namely L1-L5, connect these two α-helices and four β-strands. Each Sac10b assembles into a homodimer via an extensive hydrophobic interface and several hydrogen bonds by the residues located in helix α2, and in strands β3 and β4. The overall dimer structure of Sac10b thus adopts an architecture that gives an appearance of the letter X (referred to as Interface I). The buried surface area in this monomer-monomer interface is 755 $Å^2$ for Sac10b1 and 629 $Å^2$ for Sac10b2. Hydrophobic interactions dominate the homodimer interface between the Sac10b1 (Sac10b2) monomers. These interactions involve I45

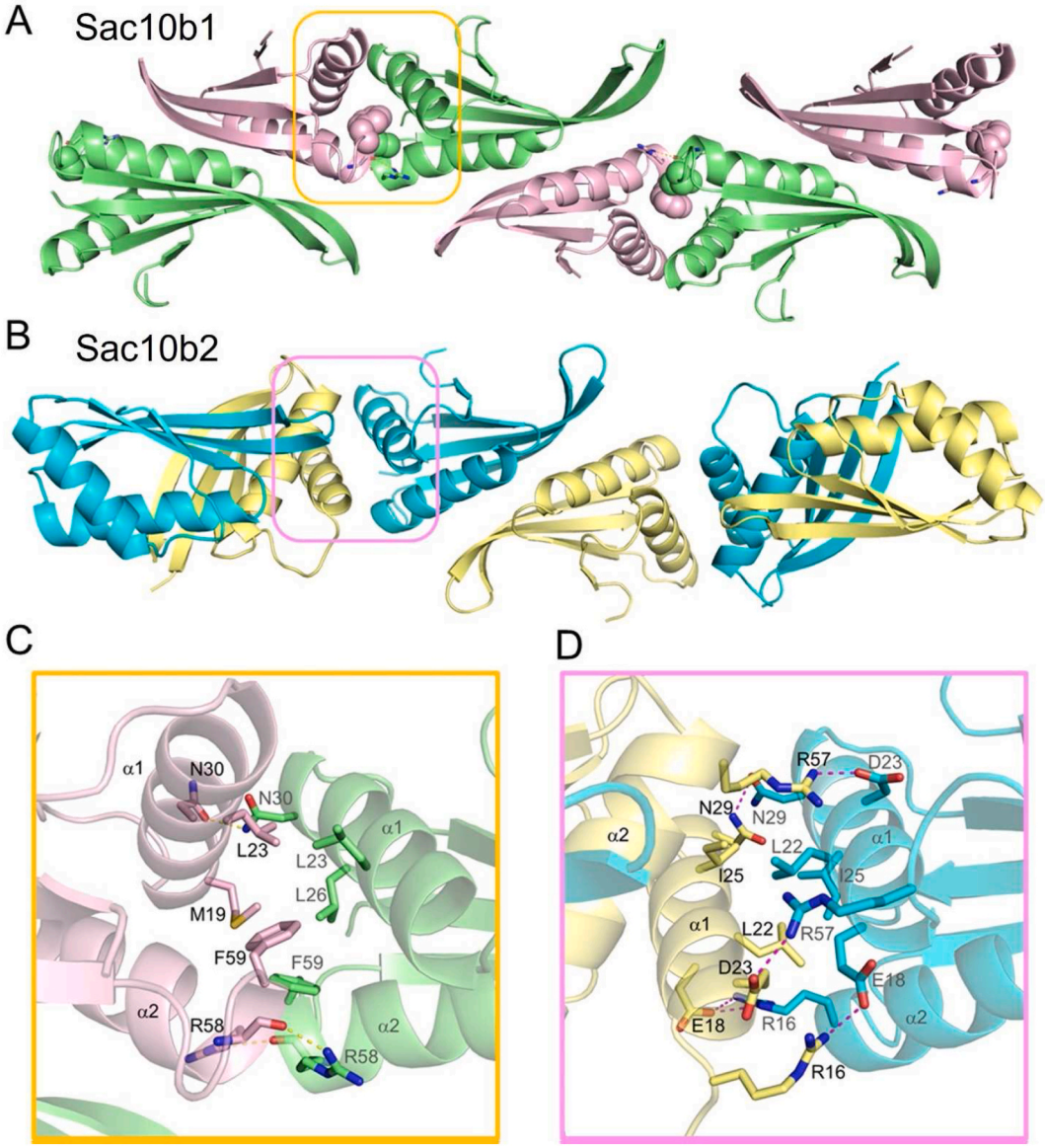

Fig. 4. Dimer-dimer interface of Sac10b. (A) The dimer-dimer interface in the Sac10b1 crystal. An end-to-end association of consecutive Sac10b1 dimers is observed in the crystal lattice. The dimer-dimer interface is marked with rectangle lines. R58 residues are shown as sticks and F59 residues are shown as spheres. (B) The dimer-dimer interface in the Sac10b2 crystal. (C) A close-up view of the dimer-dimer interface in the Sac10b1 crystal. (D) A close-up view of the dimer-dimer interface in the Sac10b2 crystal. The residues involved in dimer-dimer interactions are shown as sticks and labeled. Hydrogen bonds are indicated by dashed lines.

(I44) and V49 (I48) from α2; V66 (L64), I69 (V67), and I71 (I69) from β3; and I89 (I82) and I91 (L84) from β4 (Fig. 2C and D). Those hydrophobic interactions would be the primary driving force for dimer formation in solution. Furthermore, a few hydrogen bonding interactions appear to stabilize the contact interface of the two monomers. Hence, the polar side chains of S73 and S87 in one Sac10b1 formed hydrogen bonds with those of N57, E53, and D50 in the other and *vice versa*. In Sac10b2, the residues N45, E49, N52, R78, G70, and S80 make contacts with the other monomer by direct or water-mediated hydrogen bonds (Fig. 2A and B).

There are several salt-bridges including E35-K67, E65-R94 and D80-R82, along with an ion-pair network of E68-R70-E90 in the Sac10b1 monomer (Fig. 2E). Three salt bridges of K5-E8, K15-D23, K66-D68 and two ion-pair networks of E34-R85-E36 and R38-E72-K74 are observed in the Sac10b2 monomer (Fig. 2F). An increase in the number of salt bridges and ion-pair networks is the common feature that contributes to the thermal stability of protein at elevated temperatures [46–48]. Thermostable proteins, like Sac10b1 and Sac10b2, tend to have more ionic interactions and more extensive ion-pair networks, surpassing the average of ~5 salt bridges per 150 amino acid residues [49]. This structural evidence aligns with our CD results, indicating that both proteins exhibit high thermal stability even at temperatures as high as 95°C.

3.3. Comparison of Sac10b with structural homologues

Sac10b1 and Sac10b2 are small, dimeric proteins consisting of 97 and 90 residues per chain, respectively, and lack disulfide bonds. An amino acid sequence alignment of Sac10b family, generated using ESPript [50], is illustrated in Fig. 3A. The sequence analysis reveals that Sac10b1 and Sac10b2 share a sequence similarity of 32% identity and 58% similarity at the amino acid level. A comparison of Sac10b1-equivalent proteins from *S. acidocaldarius*, *S. tokodaii*, and *S. solfataricus* reveals a substantial 90% identity among them. In contrast, the Sac10b2 sequence exhibits only 30%–40% identity with the Sac10b1 sequence within the same species, but it displays a higher 60%–70% identity with other Sac10b2 sequences (Fig. 3A). The observed divergence in the Sac10b2 suggests a potential shift, possibly toward a novel function. However, the absence of biochemical or genetic studies has left this role unclear.

Structural comparison of the Sac10b1 and Sac10b2 proteins suggests that the characteristic features such as 3D-fold, acetylation sites, and hydrophobic inner core, are similar among the Sac10b proteins. The major differences between the two structures occur in the loop regions (Fig. 3B). In general, the loops L1, L3, and L5 play an important role in interaction with target DNA or RNA. The extended hairpin loop connecting the β3 and β4 strands is disordered in chain A of both Sac10b1 and Sac10b2, implying that this loop is highly flexible in solution. In Sac10b2, this loop contains an arginine-rich KDRRR motif (Fig. 3B), similar to the RDRRR motif in Sso10b2, which is known to be important for nucleic acid binding.

Superposition of the apo- and DNA-bound structures for different Sac10b2 homologues turns out root mean square deviations of 0.36–0.68 Å for the matched C_α atoms (Fig. 3C). Sac10b2/Sso10b2 has a short β3-β4 hairpin connected by a short turn, whereas Ape10b2 has two longer corresponding β-strands separated by a much longer loop. Interestingly, this extended hairpin loop of Ape10b2 becomes longer and more flexible upon DNA binding but does not contact the bound DNA. This structural change may play an important role in the oligomerization of Ape10b2-dimers during DNA binding to fit the incoming dimer cooperatively without steric clash [28]. In Ape10b2-DNA complex, R13 and R42 are buried within the minor groove and R86 is on the major groove side of the DNA backbone. All these three arginine residues are involved in binding to the DNA, but the corresponding residues in Sac10b2 are K13, Q42, and R77. The basic residues K74 and R77 in the loop of KDRRD motif are possible to interact with the major groove of DNA. Superposition of the apo- and RNA-bound structures for different Sac10b1 homologues gives root mean square deviations (RMSD) of 0.25–0.90 Å for the C_α atoms. Ssh10b-RNA interactions occur primarily on the loops L1 and L3 (Fig. 3D). The side chain of K16 extends into the deep major groove, and the neighboring K17 and R44 residues interact with the RNA backbone as well. These key amino acids involved in RNA binding are conserved in Sac10b1, Sso10b1, and Ssh10b.

3.4. Dimer-dimer associations in the crystal lattice

In both crystal forms of Sac10b1 and Sac10b2, dimer-dimer contacts are evident in the crystal lattice (Fig. 4). Similar to the dimerization interaction, these dimer-dimer interactions exhibit a 2-fold symmetry. The interface is predominantly shaped by anti-parallel interactions between residues in the α1 helix of one subunit of a dimer and their equivalents in another dimer. Additionally, the C-terminal end of the α2 helix is also implicated in this interaction (referred to as Interface II). In the Sac10b1 crystal, the presence of a dimer-dimer interface in the crystal lattice implies an end-to-end association of consecutive Sac10b1 dimers (Fig. 4A). Another intermolecular interface is identified between two symmetry-related dimers, characterized by a hydrophobic patch consisting of the M19, L23, L26, and F59 residues located on the surface of helices α1 and α2 (Fig. 4C). This hydrophobic patch is notably conserved in the Sac10b family. F59 plays a central role in the dimer-dimer crystallographic interface of Sac10b1, participating in a π–π stacking interaction with an adjacent dimer. In addition, one hydrogen bonding contact is observed between the N30 side chains in adjacent monomers. Two symmetric hydrogen bonds are formed between the guanidine group of R58 and its backbone carbonyl oxygen in the adjacent subunits at distances of 2.7 and 2.8 Å. These two hydrogen bonds further stabilize the hydrophobic stacking interactions between the two symmetric F59 side chains.

In the Sac10b2 crystal, the dimer-dimer association depends primarily on the interactions between two α1-helices but the end-to-end association of consecutive Sac10b2 dimers is not observed due to the absence of Sac10b1-F59-equivalent residue (Fig. 4B). In addition to hydrophobic interactions that involve L22 and I25, there are four symmetric salt-bridges between R16-E18 and R57-D23 as well as one hydrogen bond between the N29 side chains in adjacent monomers (Fig. 4D). The R57 residue of Sac10b2 does not participate in symmetric hydrogen bonds with the corresponding R57 residue in the neighboring subunit, in contrast to the interaction observed with the R58 residue in Sac10b1. Instead, R57 of Sac10b2, located in the α2 helix, establishes contact with the side chain of

D23, located in the α1 helix of the other monomer, through a salt bridge.

3.5. Sac10b1 mutation at the conserved dimer-dimer interface

The interface between dimers is highly conserved in Sac10b1 but not in Sac10b2, suggesting its crucial biological function. To probe the significance of the observed dimer-dimer contacts in crystals, mutations were introduced in Sac10b1, replacing two residues, R58 and F59, with alanine. AUC analysis of the Sac10b1 F59A protein showed an apparent molecular weight of ~20 kDa, indicating the formation of dimers in solution (Fig. 5A). In contrast, AUC of the purified Sac10b1 R58A mutant displayed higher-order oligomers of various sizes in solution with high absorbance at 260 nm (Fig. 5B). The observed oligomerization pattern in the Sac10b1 R58A mutant aligns with findings in the R10A, R13A, R46A, and R86A mutants of Ape10b2 [35], suggesting a shared tendency for oligomerization in the R58A mutant of Sac10b1. The diverse sizes of the R58A oligomers might impede crystallization, as no crystals were observed despite extensive robot screening. In contrast, F59A as a dimer in solution can form good crystals in many different crystallization conditions and most crystals belong to the *C*2 space group. The overall structure of F59A is similar to the wild-type Sac10b1, with an RMSD value of 0.486 Å for all Cα carbons in the homodimers. The principal conformational disparities between these two structures are primarily located near the mutation site at residues 59, situated at the tip of the α2-helix. Additionally, differences are observed in the relatively flexible regions of the β-hairpin arms (Fig. S2A). The dimer of F59A also formed an X-shaped quaternary structure, in which the buried surface area of this monomer-monomer interface is 738 $Å^2$. The residues S46, D50, E53, N57, S73, S87 and R85 in one monomer make contacts with the other monomer by direct or water-mediated hydrogen bonds (Fig. 6A). The homodimer interface between the F59A monomers is primarily driven by hydrophobic interactions, aligning with observations seen in the wild-type Sac10b (Fig. S2B). The 2Fo-Fc Fourier map, displaying clear electron density at the mutation site of A59, confirms the success of the mutation (Fig. S2C). The crystal packing analysis of the F59A mutant reveals a distinct dimer-dimer interface, clearly different from that observed in the wild-type Sac10b1 and Sac10b2 proteins. In the F59A crystal structure, the N83 residue (chain A) in one dimer forms hydrogen bonds with N57 (chain A) and R85 (chain B) in the other, and *vice versa* (Fig. 6B and C). In addition to the absence of π–π stacking interactions between two adjacent F59 residues, the F59A mutant exhibits notably fewer contacts at the dimer-dimer interface compared to wild-type Sac10b1. The mutant interface has a smaller surface area of 147 $Å^2$, indicating weaker interactions between two F59A dimers.

3.6. Visualizing Sac10b-DNA interactions by EM

To explore the DNA binding mechanisms of Sac10b proteins, electron microscopy was employed to directly visualize Sac10b-DNA complexes. Previous biochemical data on the interaction between Sso10b1 and DNA indicated a final stoichiometry of one Sso10b1 dimer per 6 base pairs of bound dsDNA [16,19]. Therefore, the impact of Sac10b binding to a single-nicked, circular double-stranded phiX174 plasmid of 5.4 kilo-base pairs was investigated at a ratio of 6 base pairs of DNA per protein dimer. Electron microscopy samples were prepared using cytochrome *c* spreading and rotary shadowing with tungsten for contrast enhancement [43,44]. A series of representative EM images is presented in Fig. 7 and Fig. S3. In the absence of Sac10b proteins, the relaxed phiX174 plasmid assumes a circular form (Fig. 7A). Upon binding of Sac10b1, two DNA duplexes are bridged. At a ratio of 6 base pairs per dimer, most Sac10b1-DNA complexes are bridged (90%, n = 52). Half of these bridging complexes contain single or multiple protein patches extending over part of each DNA molecule, while the other half is close to being completely bridged (45% of all DNA molecules) (Fig. 7B). These EM images of Sac10b1-DNA complexes indicate that Sac10b1 polymerizes on dsDNA molecules, forming filaments

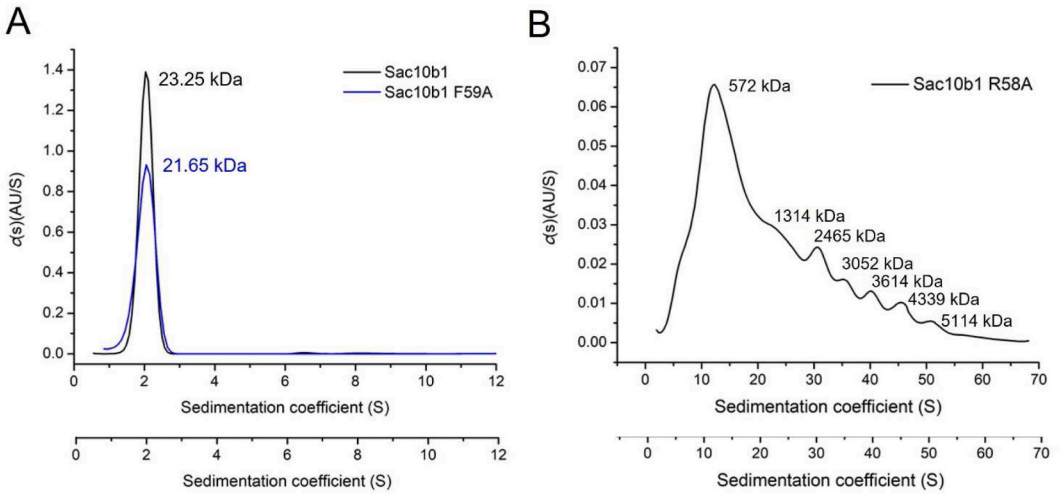

Fig. 5. AUC profiles of Sac10b1 mutants. (A) AUC profile of Sac10b1 and its mutant, F59A at 280 nm. (B) AUC profile of Sac10b1 R58A at 260 nm. The calculated molecular weight was labeled on the corresponding peak.

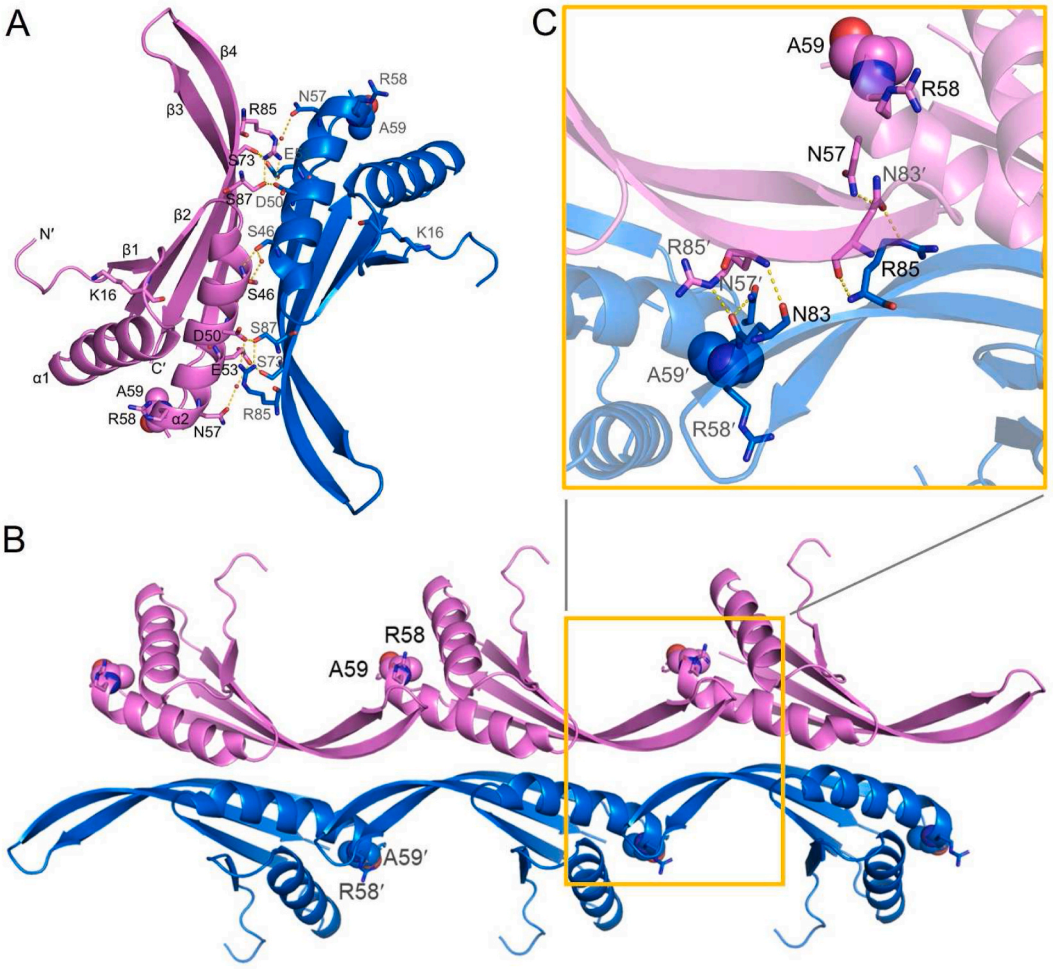

Fig. 6. Overall structures and dimer-dimer interface of Sac10b1 F59A. (A) ribbon diagram of the Sac10b1 F59A dimer is viewed along the molecular dyad axis. The subunits are colored in marine and violet. (B) The dimer-dimer interface in the crystal of Sac10b1 F59A protein. R58 residues are shown as sticks and A59 residues are shown as spheres. (C) A close-up view of the dimer-dimer interface in the Sac10b1 F59A crystal. The residues involved in dimer-dimer interactions are shown as sticks and labeled. Hydrogen bonds are indicated by dashed lines. (For interpretation of the references to color in this figure legend, the reader is referred to the Web version of this article.)

that bridge two dsDNA strands, consistent with previous observations [15,17,25]. This suggests DNA-induced cooperative binding, enhanced by the formation of stable bridges. These Sac10b1-DNA complexes resemble the bridged protein-DNA complexes observed for low-concentration Sso10b1 [25], Sso10a1 [51], and bacterial H-NS [52]. However, in contrast to Sso10b, which can either bridge or stiffen DNA based on dimer composition and concentration [25], the stiffening of DNA bound with Sac10b1 was not observed in our EM images at a ratio of 6 base pairs per protein dimer.

On the other hand, the presence of Sac10b2 dimers at similar concentrations also resulted in the development of intra-molecular bridging complexes (Fig. 7C). Within a single plasmid, the number of bridged regions by Sac10b2 is considerably fewer than those observed with Sac10b1, indicating that DNA bridging by Sac10b2 is non-cooperative. This behavior contrasts with Sac10b1, which displays cooperative binding, leading to the creation of extended bridged filaments. Similar to Sac10b2, mutations at the dimer-dimer interface of Sac10b1 (R58A and F59A) exhibit small, bridged regions in the protein-DNA complexes, and none of the complexes are fully bridged. These EM images highlight that the additional protein-protein interactions formed upon binding of wild-type Sac10b1 to longer duplexes are absent in the R58A or F59A complexes (Fig. 7D and E). This characteristic aligns with the observation in Sac10b2, where the end-to-end associations at the dimer-dimer interface are weakened or disrupted. As a result, non-cooperative binding to DNA occurs, resulting in the formation of small, bridged regions in the complex.

4. Discussion

As shown above, the dimeric Sac10b is capable of binding to DNA. Interactions between the DNA-bound Sac10b dimers should account for the bridged DNA segments. Multimeric forms of Sac10b1 and Sac10b2 have not been observed in solution by AUC,

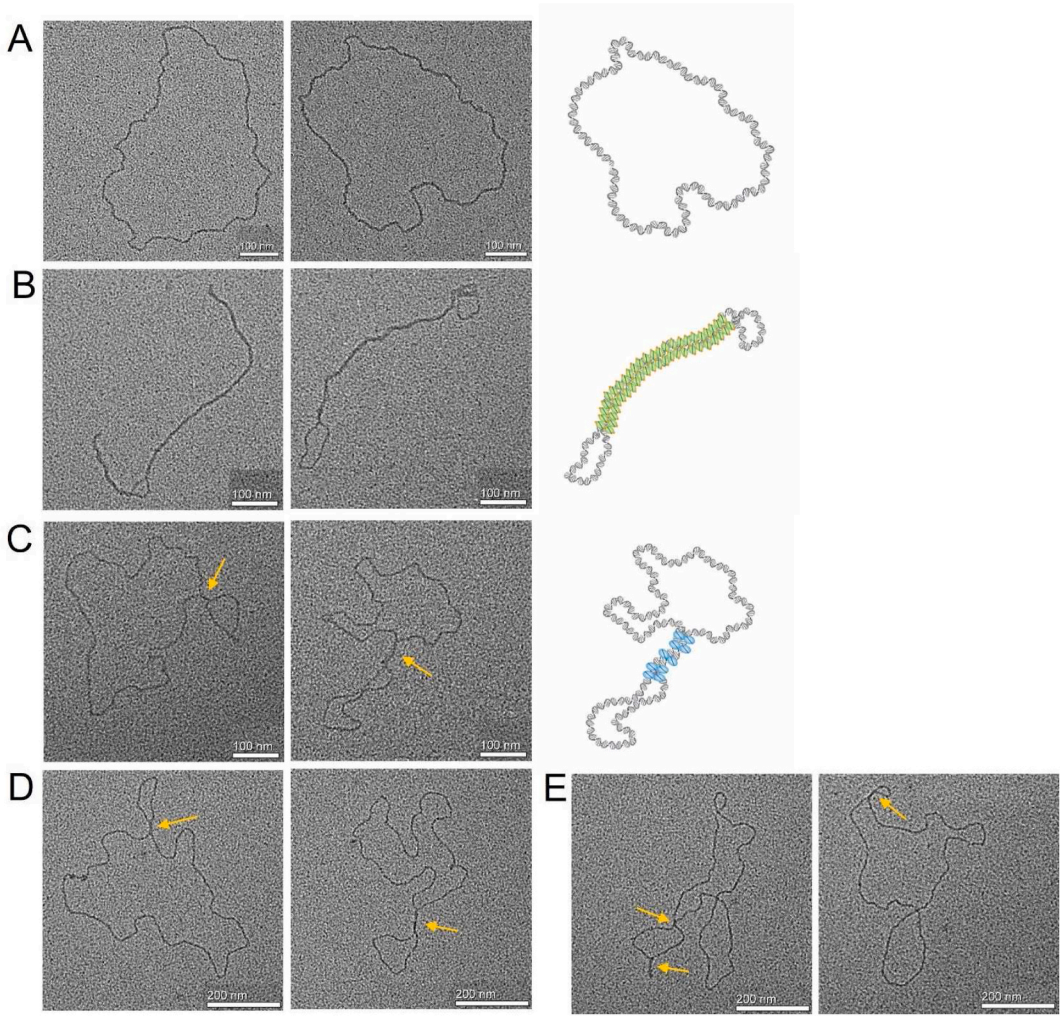

Fig. 7. Electron micrographs of nicked circular phiX174 plasmid bound with or without the Sac10b proteins. Representative images of various Sac10b-DNA complexes (6bp/dimer) visualized by EM are shown for (A) relaxed, circular phiX174 plasmid, (B) Sac10b1-DNA complex, (C) Sac10b2-DNA complex, (D) Sac10b1 R58A-DNA complex and (E) Sac10b1 F59A-DNA complex. Based on the EM images, the complexes were classified as an 'open' or a 'bridged' form. Molecules with no crossings or single DNA crossings were classified as an 'open' form. Molecules with bridged regions, of which the length is longer than a single crossover of two DNA strands, were classified as a 'bridged' form. *White scale bar*, 100 nm in (A), (B) and (C); *White scale bar*, 200 nm in (D) and (E). Each of the orange arrow points to a bridging region in the complex. In (B) and (C), green and cyan ovals indicate Sac10b1 and Sac10b2 dimers, respectively. (For interpretation of the references to color in this figure legend, the reader is referred to the Web version of this article.)

suggesting that these dimer-dimer interactions are only possible between DNA-bound Sac10b1 or DNA-bound Sac10b2 dimers. The bridging probably involves protein-protein interactions between DNA-bound protein dimers as suggested for Fis [2], a bacterial nucleoid-associated protein. On the other hand, crystal lattice packing may suggest a role of the protein-protein interfaces in forming the dimer and higher-order oligomers in solution.

In the crystals, Sac10b1 and Sac10b2 have surface areas of 755 $Å^2$ and 629 $Å^2$ buried at the dimer interface, as shown in Fig. 2A and B (Interface I). A second interface for dimer-dimer association has buried surface areas of 384 $Å^2$ in Sac10b1 and 519 $Å^2$ in Sac10b2 (Fig. 4) (Interface II). The crystal structures of Sac10b1 protein and its homologues from several species highlight a highly conserved dimer-dimer interface center on the R58 and F59 residues, which interact with their counterparts in the adjacent Sac10b1 dimer. An end-to-end association of consecutive Sac10b1 dimers is suggested by the crystal lattice (Fig. 4A). This dimer-dimer interface is stabilized by the π-π stacking interaction between the F59 side chains as well as two symmetric hydrogen bonds between the R58 residues (Fig. 4A and C).

Identical dimer-dimer interactions via the R58 and F59 residues in Sac10b1 (Fig. 8A, right) were also observed in other crystal structures of Sac10b family proteins, including Sso10b1 [35] and Afu10b1 [35]. These interactions at the interface have biological relevance that may relate to the formation of extended bridged filament as observed by EM. Upon binding to dsDNA, excess Sac10b1 formed an extended bridged filament, most likely through the continuous association of Sac10b1 dimers. This dimer-dimer contact is

also present in the structure of Ape10b2-DNA complex [35], where the crystal lattice of the complex shows that the array of proteins packs above and below the dsDNA (Fig. 8A, left). A recent NMR analysis of R59 and F60 in Sso10b1 [26], corresponding to R57 and F58 in Ape10b2 [35] and R58 and F59 in Sac10b1, revealed the significance of these residues in multimerization and protein-DNA interaction.

Sequence conservation analysis of the Sac10b (Alba) protein family from Archaea (Fig. S4 and Fig. 3A) reveals significant conservation, particularly at positions R58 and F59. This suggests a critical role for these specific residues in Sac10b function. Furthermore, biochemical and structural studies have identified multiple conserved amino acids across the Sac10b family (K15, K16, Y21, R41, R43, R82, etc., in Sac10b1) that are likely involved in nucleic acid binding. Notably, the conservation of K16 (K17 in Sis10b), a residue known to be essential for RNA binding and chaperone activity in other Sac10b family members, suggests that Sac10b may also possess similar RNA-related functions [23].

Based on structural insights and biochemical data, the dimer-dimer contact appears to be a pivotal factor in bringing together multiple extended bridged fibers in the Sac10b-DNA complex during DNA packaging. Consequently, we propose a model of Sac10b1-

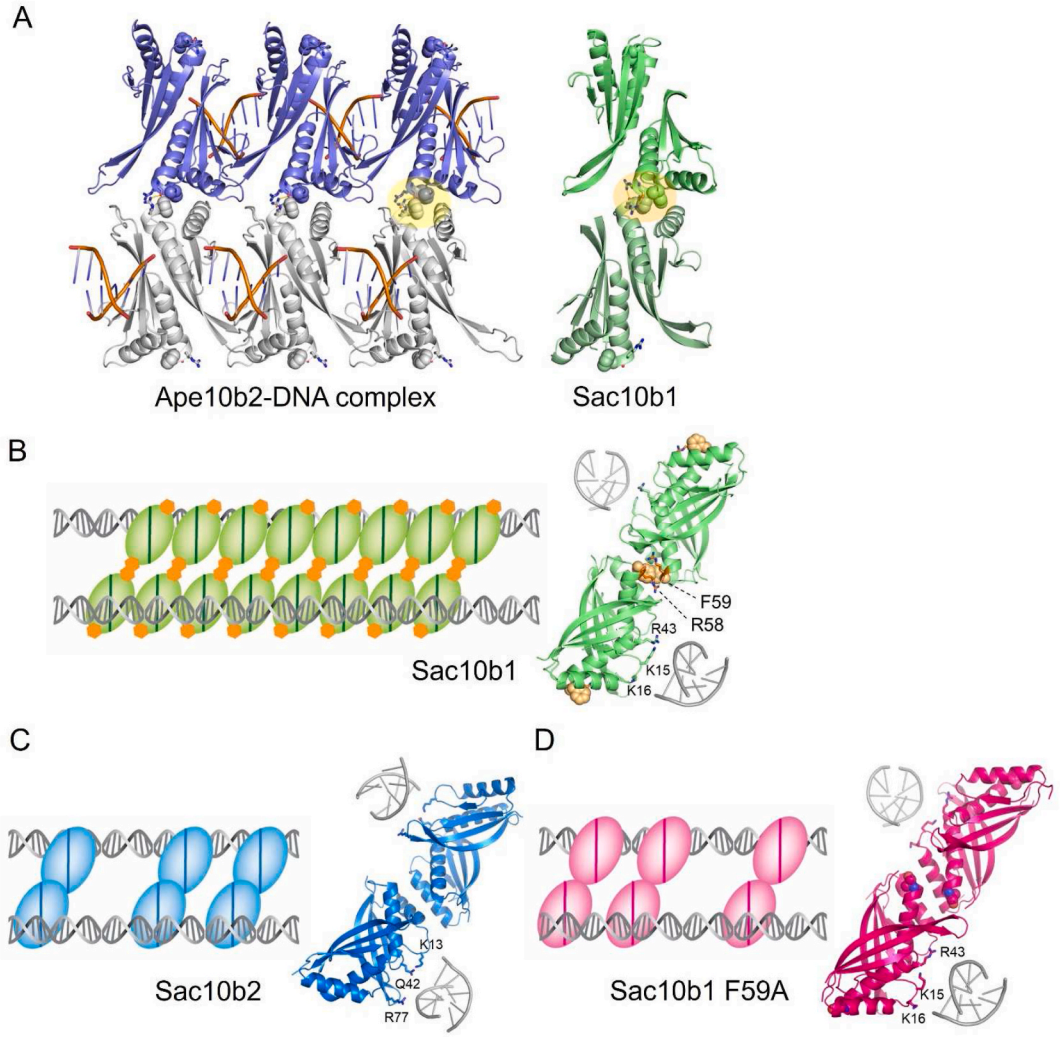

Fig. 8. Bridged DNA structure mediated by dimer-dimer association. (A) Oligomerization of Ape10b2-DNA complex (PDB ID: 3U6Y) in the crystal lattice (Left, two dimers are colored in slate and grey). The crystal packing diagrams show that the dimer-dimer interactions between two Sac10b1 dimers (Right, transparent orange oval) have also been found in the crystal of Ape10b2-DNA complex (Left, transparent yellow oval). (B) Model of Sac10b1-DNA bridging interaction. Each Sac10b1 dimer (color in green) interacts with DNA via the K15, K16 and R43 residues, which are shown as sticks. The two Sac10b1-DNA duplexes are bridged by the end-to-end interactions of the two α2-helices, including the contacts between the symmetry-related F59 residues (shown as orange spheres) and R58 residues (shown as orange sticks). (C) Model of Sac10b2-DNA bridging interaction. Each Sac10b2 dimer (colored in marine) interacts with DNA via the K13, Q42 and R77 residues, which are shown as sticks. (D) Model of Sac10b1 F59A-DNA bridging interaction. The Sac10b1 F59A dimers (colored in hot pink) exhibit non-cooperative binding along the DNA, and so does R58A. Bridges can be formed by both mutants but are less stable compared with the wild-type Sac10b1 bridges. (For interpretation of the references to color in this figure legend, the reader is referred to the Web version of this article.)

DNA, Sac10b2-DNA, and Sac10b1 F59A-DNA bridging interactions, drawing upon the structural information from Sac10b1, Sac10b2, and Sac10b1 F59A, aligned with the Ape10b2-dsDNA complex [35] (Fig. 8B-D). In the Sac10b1-DNA model, the cooperative binding of Sac10b1 to DNA, facilitated by dimer-dimer association, is mediated by the residues R58 and F59 (Fig. 8B). Sac10b1 can interact with other dimers on an adjacent DNA duplex, resulting in the formation of a bridged structure. An intriguing hypothesis is that the dimer-dimer interface may serve as a pathway through which DNA could be rapidly packed into high-order structures via these bridging interactions.

In the crystal structure of Sac10b2, the dimer-dimer association primarily relies on interactions between the two α1-helices. However, the end-to-end association of consecutive Sac10b2 dimers via R58 and L59 is absent due to the lack of an F59-equivalent residue (Fig. 4B). Similarly, it has been proposed that the function of Sso10b2 is to weaken or disrupt the dimer-dimer interface in protein fibers [17]. The conserved F59 dimer-dimer interface is absent in the Sso10b1 F59A crystal. The dimer-dimer interactions in Sac10b2 along a single DNA duplex are limited to separate contacts between two dimers, resulting in the observation of only a small bridged complex in our EM images. The previous studies on Sso10b1 [25,26] and our investigations on Sac10b1 have demonstrated the crucial role of the phenylalanine side chain in dimer-dimer stacking and the promotion of cooperative binding to dsDNA. Furthermore, our findings suggest that the R58 residue is also essential for cooperative binding and DNA bridging.

Based on the findings from these studies, it appears that dimer-dimer interactions in Sac10b proteins play a crucial role in bringing together two DNA duplexes. The observed differences in DNA bridging between Sac10b1 and Sac10b2 can likely be attributed to variations in dimer-dimer interactions. The interaction surface is highly conserved in Sac10b1, but not in Sac10b2. Intriguingly, cooperative binding to DNA is influenced by mutating the R58 and F59 residues. The impact of Sac10b2 on DNA resembles that of the Sac10b1 R58A and Sac10b1 F59A mutants, resulting in a reduction in the extent of DNA bridging. Taken together, these studies suggest that both the R58 and F59 residues play an indispensable role in facilitating cooperative binding and DNA bridging, contributing to the formation of densely packed protein-DNA filaments.

Furthermore, the noted variations in DNA affinity and bridging tendencies between the closely related proteins Sac10b1 and Sac10b2 within the same organism strongly suggest a potential regulatory mechanism. The distinct DNA bridging interactions exhibited by Sac10b2, as opposed to Sac10b1, indicate that organisms may modulate chromatin structure in response to environmental or growth conditions through selective expression of these proteins. A similar phenomenon has been observed for the archaeal histone proteins, in which the histones HMfA and HMfB are differentially expressed during the growth phase of the *M. fervidus*, with the latter protein providing a higher level of compaction of DNA [53]. These data suggest that both Sac10b proteins can perform a DNA bridging function in different ways to help the organization and stabilization of the genomic DNA in archaea under extreme conditions.

In bacteria, the DNA-bridging interaction is likely involved in forming higher-order looped structures representing topologically isolated domains and the formation of these domains has been attributed to bridging/looping by H-NS [2]. The DNA within these domains is additionally compacted due to the presence of supercoils. Although higher-order organization of archaeal genomes has not been explicitly addressed to date, it is speculated that crenarchaea DNA may exhibit an organization in looped domains similar to that found in bacteria, where a key role of chromosomal proteins is envisioned for bridging and bending the DNA [1,3,4,54,55]. For example, DNA bending induced by proteins such as Sul7 (e.g., Sac7d and Sso7d) and Cren7 can facilitate the formation of small loops through interaction with a DNA bridging protein like Sac10b. Originally, the focus in archaea was on how proteins like Sso10b and Cren7 collaborate to regulate chromatin compaction through their independent and synergistic interactions with DNA [56]. This concept of cooperative DNA binding has inspired researchers in cancer therapy to explore the potential of small molecule drugs exhibiting similar synergy. The rationale lies in the promise of developing more potent treatments through such synergistic interactions [57–59]. A recent study exemplifies this approach by investigating the structural mechanisms employed by two DNA-intercalating drugs when they synergistically target mismatched DNA, leading to specific alterations in the DNA backbone [58,59]. These insights not only hold value for this particular drug combination but also offer a broader perspective for understanding the formation of other protein-DNA and drug-DNA complexes.

5. Conclusion

This study sheds light on the intricate interactions between Sac10b proteins and DNA in archaea, focusing on cooperative binding and bridging mechanisms. Identifying critical residues and characterizing dimer-dimer interfaces significantly advances our understanding of how Sac10b proteins organize and stabilize genomic DNA. Observed variations in DNA interaction between Sac10b1 and Sac10b2 suggest potential regulatory roles in response to specific growth or environmental cues. A proposed model for Sac10b-DNA interactions and potential synergy with other DNA-binding proteins establishes a framework for future investigations into archaeal chromosomal organization. In essence, this research provides valuable insights into both the structure and function of Sac10b proteins, paving the way for further exploration of dynamic genetic material regulation in extremophiles.

Data availability

The atomic coordinates have been deposited in the Protein Data Bank under accession code 8XAO for Sac10b1, 8XAP for Sac10b2 and 8XAQ for Sac10b1 F59A.

CRediT authorship contribution statement

Songqiang Tang: Validation, Investigation, Data curation. **Chun-Hsiang Huang:** Validation, Investigation, Formal analysis, Data

curation. **Tzu-Ping Ko:** Writing – review & editing, Writing – original draft. **Kuan-Fu Lin:** Validation, Investigation. **Yuan-Chih Chang:** Investigation. **Po-Yen Lin:** Investigation. **Liuchang Sun:** Visualization, Validation, Investigation. **Chin-Yu Chen:** Writing – review & editing, Writing – original draft, Supervision, Funding acquisition, Conceptualization.

Declaration of competing interest

The authors declare that they have no known competing financial interests or personal relationships that could have appeared to influence the work reported in this paper.

Acknowledgments

This work was supported by National Natural Sciences Foundation of China (U22A20551) and major scientific and technological projects in Hubei Province (2023BBA002). The authors gratefully acknowledge the technical services provided by the National Synchrotron Radiation Research Center (NSRRC), supported by the Ministry of Science and Technology of Taiwan. The EM experiments were performed at the Academia Sinica Cryo-EM Facility (ASCEM). ASCEM is supported by Academia Sinica Core Facility and Innovative Instrument Project (AS-CFII-111-210).

Appendix A. Supplementary data

Supplementary data to this article can be found online at https://doi.org/10.1016/j.heliyon.2024.e31630.

References

[1] M.S. Luijsterburg, M.F. White, R. Van Driel, R. Th Dame, The major architects of chromatin: architectural proteins in bacteria, archaea and eukaryotes, Crit. Rev. Biochem. Mol. Biol. 43 (2008) 393–418, https://doi.org/10.1080/10409230802528488.
[2] S.C. Dillon, C.J. Dorman, Bacterial nucleoid-associated proteins, nucleoid structure and gene expression, Nat. Rev. Microbiol. 8 (2010) 185–195, https://doi.org/10.1038/nrmicro2261.
[3] R.P.C. Driessen, R.T. Dame, Nucleoid-associated proteins in crenarchaea, Biochem. Soc. Trans. 39 (2011) 116–121, https://doi.org/10.1042/BST0390116.
[4] M.F. White, S.D. Bell, Holding it together: chromatin in the Archaea, Trends Genet. 18 (2002) 621–626, https://doi.org/10.1016/S0168-9525(02)02808-1.
[5] K. Sandman, J.N. Reeve, Archaeal chromatin proteins: different structures but common function? Curr. Opin. Microbiol. 8 (2005) 656–661, https://doi.org/10.1016/j.mib.2005.10.007.
[6] J.N. Reeve, K.A. Bailey, W. Li, F. Marc, K. Sandman, D.J. Soares, Archaeal histones: structures, stability and DNA binding, Biochem. Soc. Trans. 32 (2004) 227–230, https://doi.org/10.1042/BST0320227.
[7] H. Maruyama, J.C. Harwood, K.M. Moore, K. Paszkiewicz, S.C. Durley, H. Fukushima, H. Atomi, K. Takeyasu, N.A. Kent, An alternative beads-on-a-string chromatin architecture in *Thermococcus kodakarensis*, EMBO Rep. 14 (2013) 711–717, https://doi.org/10.1038/embor.2013.94.
[8] B. Henneman, R.T. Dame, Archaeal histones: dynamic and versatile genome architects, AIMS Microbiol 1 (2015) 72–81, https://doi.org/10.3934/microbiol.2015.1.72.
[9] F. Mattiroli, S. Bhattacharyya, P.N. Dyer, A.E. White, K. Sandman, B.W. Burkhart, K.R. Byrne, T. Lee, N.G. Ahn, T.J. Santangelo, J.N. Reeve, K. Luger, Structure of histone-based chromatin in Archaea, Science 357 (2017) (1979) 609–612, https://doi.org/10.1126/science.aaj1849.
[10] S. Ofer, F. Blombach, A.M. Erkelens, D. Barker, Z. Soloviev, S. Schwab, K. Smollett, D. Matelska, T. Fouqueau, N. van der Vis, N.A. Kent, K. Thalassinos, R. T. Dame, F. Werner, DNA-bridging by an archaeal histone variant via a unique tetramerisation interface, Commun. Biol. 6 (2023), https://doi.org/10.1038/s42003-023-05348-2.
[11] J. Xuan, Y. Feng, The archaeal Sac10b protein family: conserved proteins with divergent functions, Curr. Protein Pept. Sci. 13 (2012) 258–266, https://doi.org/10.2174/138920312800785067.
[12] M. Goyal, C. Banerjee, S. Nag, U. Bandyopadhyay, The Alba protein family: structure and function, Biochim. Biophys. Acta, Proteins Proteomics 1864 (2016) 570–583, https://doi.org/10.1016/j.bbapap.2016.02.015.
[13] G.R. Green, D.G. Searcy, R.J. DeLange, Histone-like protein in the archaebacterium *Sulfolobus acidocaldarius*, Biochim. Biophys. Acta Gene Struct. Expr. 741 (1983) 251–257, https://doi.org/10.1016/0167-4781(83)90066-0.
[14] M. Grote, J. Dijk, R. Reinhardt, Ribosomal and DNA binding proteins of the thermoacidophilic archaebacterium *Sulfolobus acidocaldarius*, Biochim. Biophys. Acta Protein Struct. Mol. Enzymol. 873 (1986) 405–413, https://doi.org/10.1016/0167-4838(86)90090-7.
[15] R. Lurz, M. Grote, J. Dijk, R. Reinhardt, B. Dobrinski, Electron microscopic study of DNA complexes with proteins from the Archaebacterium *Sulfolobus acidocaldarius*, EMBO J. 5 (1986) 3715–3721. http://www.ncbi.nlm.nih.gov/pmc/articles/PMC1167416/.
[16] B.N. Wardleworth, R.J.M. Russell, S.D. Bell, G.L. Taylor, M.F. White, Structure of Alba: an archaeal chromatin protein modulated by acetylation, EMBO J. 21 (2002) 4654–4662, https://doi.org/10.1093/emboj/cdf465.
[17] C. Jelinska, M.J. Conroy, C.J. Craven, A.M. Hounslow, P.A. Bullough, J.P. Waltho, G.L. Taylor, M.F. White, Obligate heterodimerization of the archaeal Alba2 protein with Alba1 provides a mechanism for control of DNA packaging, Structure 13 (2005) 963–971, https://doi.org/10.1016/j.str.2005.04.016.
[18] S.D. Bell, C.H. Botting, B.N. Wardleworth, S.P. Jackson, M.F. White, The interaction of Alba, a conserved archaeal chromatin protein, with Sir2 and its regulation by acetylation, Science 296 (2002) (1979) 148–151, https://doi.org/10.1126/science.1070506.
[19] H. Xue, R. Guo, Y. Wen, D. Liu, L. Huang, An abundant DNA binding protein from the hyperthermophilic archaeon *Sulfolobus shibatae* affects DNA supercoiling in a temperature-dependent fashion, J. Bacteriol. 182 (2000) 3929–3933, https://doi.org/10.1128/JB.182.14.3929-3933.2000.
[20] R. Guo, H. Xue, L. Huang, Ssh10b, a conserved thermophilic archaeal protein, binds RNA in vivo, Mol. Microbiol. 50 (2003) 1605–1615, https://doi.org/10.1046/j.1365-2958.2003.03793.x.
[21] Q. Cui, Y. Tong, H. Xue, L. Huang, Y. Feng, J. Wang, Two conformations of archaeal Ssh10b: the origin of its temperature-dependent interaction with DNA, J. Biol. Chem. 278 (2003) 51015–51022, https://doi.org/10.1074/jbc.M308510200.
[22] J. Cao, Q. Wang, T. Liu, N. Peng, L. Huang, Insights into the post-translational modifications of archaeal Sis10b (Alba): lysine-16 is methylated, not acetylated, and this does not regulate transcription or growth, Mol. Microbiol. 109 (2018) 192–208, https://doi.org/10.1111/mmi.13973.
[23] N. Zhang, L. Guo, L. Huang, The Sac10b homolog from *Sulfolobus islandicus* is an RNA chaperone, Nucleic Acids Res. 48 (2020) 9273–9284, https://doi.org/10.1093/nar/gkaa656.

[24] M. Črnigoj, Z. Podlesek, M. Zorko, R. Jerala, G. Anderluh, N.P. Ulrih, Interactions of archaeal chromatin proteins Alba1 and Alba2 with nucleic acids, PLoS One 8 (2013) e58237, https://doi.org/10.1371/journal.pone.0058237.

[25] N. Laurens, R.P.C. Driessen, I. Heller, D. Vorselen, M.C. Noom, F.J.H. Hol, M.F. White, R.T. Dame, G.J.L. Wuite, Alba shapes the archaeal genome using a delicate balance of bridging and stiffening the DNA, Nat. Commun. 3 (2012) 1328, https://doi.org/10.1038/ncomms2330.

[26] C. Jelinska, B. Petrovic-Stojanovska, W.J. Ingledew, M.F. White, Dimer-dimer stacking interactions are important for nucleic acid binding by the archaeal chromatin protein Alba, Biochem. J. 427 (2010) 49–55, https://doi.org/10.1042/BJ20091841.

[27] V.L. Marsh, S.Y. Peak-Chew, S.D. Bell, Sir2 and the acetyltransferase, Pat, regulate the archaeal chromatin protein, Alba, J. Biol. Chem. 280 (2005) 21122–21128, https://doi.org/10.1074/jbc.M501280200.

[28] L. Guo, J. Ding, R. Guo, Y. Hou, D.C. Wang, L. Huang, Biochemical and structural insights into RNA binding by Ssh10b, a member of the highly conserved Sac10b protein family in archaea, J. Biol. Chem. 289 (2014) 1478–1490, https://doi.org/10.1074/jbc.M113.521351.

[29] C.C. Chou, T.W. Lin, C.Y. Chen, A.H.J. Wang, Crystal structure of the hyperthermophilic archaeal DNA-binding protein Sso10b2 at a resolution of 1.85 Angstroms, J. Bacteriol. 185 (2003) 4066–4073, https://doi.org/10.1128/JB.185.14.4066-4073.2003.

[30] T. Kumarevel, K. Sakamoto, S.C.B. Gopinath, A. Shinkai, P.K.R. Kumar, S. Yokoyama, Crystal structure of an archaeal specific DNA-binding protein (Ape10b2) from *Aeropyrum pernix* K1, Proteins: structure, Function and Genetics 71 (2008) 1156–1162, https://doi.org/10.1002/prot.21807.

[31] G. Wang, R. Guo, M. Bartlam, H. Yang, H. Xue, Y. Liu, L. Huang, Z. Rao, Crystal structure of a DNA binding protein from the hyperthermophilic euryarchaeon *Methanococcus jannaschii*, Protein Sci. 12 (2003) 2815–2822, https://doi.org/10.1110/ps.03325103.

[32] K. Zhao, X. Chai, R. Marmorstein, Structure of a Sir2 substrate, Alba, reveals a mechanism for deacetylation-induced enhancement of DNA binding, J. Biol. Chem. 278 (2003) 26071–26077, https://doi.org/10.1074/jbc.M303666200.

[33] K. Hada, T. Nakashima, T. Osawa, H. Shimada, Y. Kakuta, M. Kimura, Crystal structure and functional analysis of an archaeal chromatin protein alba from the hyperthermophilic archaeon *Pyrococcus horikoshii* OT3, Biosci. Biotechnol. Biochem. 72 (2008) 749–758, https://doi.org/10.1271/bbb.70639.

[34] Y.-F. Liu, N. Zhang, X. Liu, X. Wang, Z.-X. Wang, Y. Chen, H.-W. Yao, M. Ge, X.-M. Pan, Molecular mechanism underlying the interaction of typical Sac10b family proteins with DNA, PLoS One 7 (2012) e34986, https://doi.org/10.1371/journal.pone.0034986.

[35] T. Tanaka, S. Padavattan, T. Kumarevel, Crystal structure of archaeal chromatin protein alba2-double-stranded DNA complex from *Aeropyrum pernix* K1, J. Biol. Chem. 287 (2012) 10394–10402, https://doi.org/10.1074/jbc.M112.343210.

[36] Q. Cui, Y. Tong, H. Xue, L. Huang, Y. Feng, J. Wang, Two conformations of archaeal Ssh10b: the origin of its temperature-dependent interaction with DNA, J. Biol. Chem. 278 (2003) 51015–51022, https://doi.org/10.1074/jbc.M308510200.

[37] P. Schuck, Size-distribution analysis of macromolecules by sedimentation velocity ultracentrifugation and Lamm equation modeling, Biophys. J. 78 (2000) 1606–1619, https://doi.org/10.1016/S0006-3495(00)76713-0.

[38] Z. Otwinowski, W. Minor, Processing of X-ray diffraction data collected in oscillation mode, Methods Enzymol. 276 (1997) 307–326.

[39] A.J. McCoy, R.W. Grosse-Kunstleve, P.D. Adams, M.D. Winn, L.C. Storoni, R.J. Read, Phaser crystallographic software, J. Appl. Crystallogr. 40 (2007) 658–674, https://doi.org/10.1107/S0021889807021206.

[40] P. Emsley, B. Lohkamp, W.G. Scott, K. Cowtan, Features and development of Coot, Acta Crystallogr D Biol Crystallogr 66 (2010) 486–501, https://doi.org/10.1107/S0907444910007493.

[41] P.D. Adams, P.V. Afonine, G. Bunkóczi, V.B. Chen, I.W. Davis, N. Echols, J.J. Headd, L.W. Hung, G.J. Kapral, R.W. Grosse-Kunstleve, A.J. McCoy, N.W. Moriarty, R. Oeffner, R.J. Read, D.C. Richardson, J.S. Richardson, T.C. Terwilliger, P.H. Zwart, PHENIX: a comprehensive Python-based system for macromolecular structure solution, Acta Crystallogr D Biol Crystallogr 66 (2010) 213–221, https://doi.org/10.1107/S0907444909052925.

[42] V.B. Chen, W.B. Arendall, J.J. Headd, D.A. Keedy, R.M. Immormino, G.J. Kapral, L.W. Murray, J.S. Richardson, D.C. Richardson, MolProbity: all-atom structure validation for macromolecular crystallography, Acta Crystallogr D Biol Crystallogr 66 (2010) 12–21, https://doi.org/10.1107/S0907444909042073.

[43] J.D. Griffith, G. Christiansen, Electron microscope visualization of chromatin and other DNA-protein complexes, Annu. Rev. Biophys. Bioeng. 7 (1978) 19–35, https://doi.org/10.1146/annurev.bb.07.060178.000315.

[44] C.-T. Bock, S. Franz, H. Zentgraf, J. Sommerville, Electron microscopy of Biomolecules, in: Encyclopedia of Molecular Cell Biology and Molecular Medicine, Wiley-VCH Verlag GmbH & Co. KGaA, 2006, https://doi.org/10.1002/3527600906.mcb.200300057.

[45] K. Biyani, M.A. Kahsai, A.T. Clark, T.L. Armstrong, S.P. Edmondson, J.W. Shriver, Solution structure, stability, and nucleic acid binding of the hyperthermophile protein Sso10b2, Biochemistry 44 (2005) 14217–14230, https://doi.org/10.1021/bi051266r.

[46] A. Karshikoff, R. Ladenstein, Ion pairs and the thermotolerance of proteins from hyperthermophiles: a “traffic rule” for hot roads, Trends Biochem. Sci. 26 (2001) 550–557, https://doi.org/10.1016/S0968-0004(01)01918-1.

[47] M. Ge, X.Y. Xia, X.M. Pan, Salt bridges in the hyperthermophilic protein Ssh10b are resilient to temperature increases, J. Biol. Chem. 283 (2008) 31690–31696, https://doi.org/10.1074/jbc.M805750200.

[48] A. Szilágyi, P. Závodszky, Structural differences between mesophilic, moderately thermophilic and extremely thermophilic protein subunits: results of a comprehensive survey, Structure 8 (2000) 493–504, https://doi.org/10.1016/S0969-2126(00)00133-7.

[49] D.J. Barlow, J.M. Thornton, Ion-pairs in proteins, J. Mol. Biol. 168 (1983) 867–885, https://doi.org/10.1016/S0022-2836(83)80079-5.

[50] X. Robert, P. Gouet, Deciphering key features in protein structures with the new ENDscript server, Nucleic Acids Res. 42 (2014) 320–324, https://doi.org/10.1093/nar/gku316.

[51] R.P.C. Driessen, S.N. Lin, W.J. Waterreus, A.L.H. Van Der Meulen, R.A. Van Der Valk, N. Laurens, G.F. Moolenaar, N.S. Pannu, G.J.L. Wuite, N. Goosen, R. T. Dame, Diverse architectural properties of Sso10a proteins: evidence for a role in chromatin compaction and organization, Sci. Rep. 6 (2016) 29422, https://doi.org/10.1038/srep29422.

[52] R.T. Dame, C. Wyman, N. Goosen, H-NS mediated compaction of DNA visualised by atomic force microscopy, Nucleic Acids Res. 28 (2000) 3504–3510, https://doi.org/10.1093/nar/28.18.3504.

[53] K. Sandman, R.A. Grayling, B. Dobrinski, R. Lurz, J.N. Reeve, Growth-phase-dependent synthesis of histones in the archaeon *Methanothermus fervidus*, Proc. Natl. Acad. Sci. U. S. A. 91 (1994) 12624–12628, https://doi.org/10.1073/pnas.91.26.12624.

[54] C.H. Hsu, A.H.-J. Wang, The DNA-recognition fold of Sso7c4 suggests a new member of SpoVT-AbrB superfamily from archaea, Nucleic Acids Res. 39 (2011) 6764–6774, https://doi.org/10.1093/nar/gkr283.

[55] B.L. Lin, C.Y. Chen, C.H. Huang, T.P. Ko, C.H. Chiang, K.F. Lin, Y.C. Chang, P.Y. Lin, H.H.G. Tsai, A.H.J. Wang, The arginine pairs and C-termini of the Sso7c4 from *Sulfolobus solfataricus* participate in binding and bending DNA, PLoS One 12 (2017) 1–25, https://doi.org/10.1371/journal.pone.0169627.

[56] M.K.M. Cajili, E.I. Prieto, Interplay between Alba and Cren7 regulates chromatin compaction in *Sulfolobus solfataricus*, Biomolecules 12 (2022) 481, https://doi.org/10.3390/biom12040481.

[57] M.M. Alruwaili, J. Zonneville, M.N. Naranjo, H. Serio, T. Melendy, R.M. Straubinger, B. Gillard, B.A. Foster, P. Rajan, K. Attwood, S. Chatley, R. Iyer, C. Fountzilas, A.V. Bakin, A synergistic two-drug therapy specifically targets a DNA repair dysregulation that occurs in p53-deficient colorectal and pancreatic cancers, Cell Reports Medicine 5 (2024) 101434, https://doi.org/10.1016/j.xcrm.2024.101434.

[58] R. Satange, S.-H. Kao, C.-M. Chien, S.-H. Chou, C.-C. Lin, S. Neidle, M.-H. Hou, Staggered intercalation of DNA duplexes with base-pair modulation by two distinct drug molecules induces asymmetric backbone twisting and structure polymorphism, Nucleic Acids Res. 50 (2022) 8867–8881, https://doi.org/10.1093/nar/gkac629.

[59] R. Satange, C.-C. Chang, L.-Y. Li, S.-H. Lin, S. Neidle, M.-H. Hou, Synergistic binding of actinomycin D and echinomycin to DNA mismatch sites and their combined anti-tumour effects, Nucleic Acids Res. 51 (2023) 3540–3555, https://doi.org/10.1093/nar/gkad156.